Available online at www.sciencedirect.com
ScienceDirect
Journal of the European Ceramic Society 27 (2007) 3351–3357
www.elsevier.com/locate/jeurceramsoc

Microstructural design of sliding-wear-resistant liquid-phase-sintered SiC: An overview

Oscar Borrero-López [a], Angel L. Ortiz [a], Fernando Guiberteau [a,*], Nitin P. Padture [b]

[a] *Departamento de Electrónica e Ingeniería Electromecánica, Escuela de Ingenierías Industriales, Universidad de Extremadura, 06071 Badajoz, Spain*
[b] *Department of Materials Science and Engineering, The Ohio State University, Columbus, OH 43210, USA*

Available online 3 April 2007

Abstract

We have reviewed the effect of microstructure – content of intergranular phase, grain size, and grain shape – on the lubricated, sliding-wear of pressureless liquid-phase-sintered (LPS) SiC ceramics. The sliding-wear resistance in LPS SiC decreases with an increase in the content of the intergranular phase or an increase in the equiaxed-grain coarsening. However, the sliding-wear resistance is dramatically improved with anisotropic-grain coarsening. Based on these results we suggest two strategies for the microstructural design of low-cost, sliding-wear resistant SiC-based ceramics: (1) grain refinement, and (2) grain elongation. The latter strategy allows the materials to be simultaneously *in situ* toughened, and we describe its optimization by judicious selection of the SiC starting powder.

Keywords: Wear resistance; SiC; Sintering; Liquid-phase sintering; Microstructure

1. Introduction

Ceramics are innately hard and stiff, which makes them very attractive materials for use in contact-mechanical and tribological applications. In addition, due to their high-temperature tolerance and chemical inertness, many ceramics are appropriate for applications where lightness and/or resistance to hostile environments are required. It is not surprising then that many tribocomponents – such as bearings, wear-parts, valves, seals, rollers, cutting tools, nozzles, dies, gears, tappets, etc. – are increasingly being made of ceramics.

In this context, silicon carbide (SiC), which has one of the highest hardnesses of all single-phase ceramics, has been identified as a promising candidate for its use in the above applications.[1–8] What distinguishes SiC from the majority of the ultra-hard ceramics is its high thermal conductivity[9] and high melting point,[10] which help to relieve and resist the frictional heating in sliding contacts. However, conventional solid-state sintering of SiC bulk ceramics involves the use of extremely high temperatures and pressures, which makes SiC tribocomponents expensive, at the same time as imposing severe restrictions on their shapes and sizes. Fortunately, pressureless liquid-phase sintering enables the limitations of solid-state sintering to be overcome, paving the way towards low-cost processing of SiC ceramics. Hence, it is not surprising that liquid-phase-sintered (LPS) SiC has recently been investigated (although as yet not extensively) for its potential as a low-cost, highly sliding-wear resistant, ceramic.[7,8,11–14]

The design of SiC-based tribocomponents with improved performance requires their microstructure–properties relationship to be established. In this paper we review the effect of the microstructure on the lubricated sliding-wear of LPS SiC ceramics under initial elastic contact, in an effort to provide guidelines for the processing of low-cost SiC ceramics with tailored contact-mechanical and tribological properties.

2. Experimental procedure

2.1. Processing

Four powder batches were individually prepared, each containing α-SiC (UF-15, H.C. Stark, Germany) or β-SiC (Ultrafine SiC, Ibiden Corp., Ogaki, Japan) powder, plus a combination of Al_2O_3 (AKP-30, Sumitomo Chemical Company, New York, NY) and Y_2O_3 (Fine Grade, H.C. Starck Inc., Newton, MA) powders in the molar ratio Y_2O_3:Al_2O_3::3:5 to result in YAG

* Corresponding author. Tel.: +34 924 28 9530; fax: +34 924 289601.
E-mail address: guiberto@unex.es (F. Guiberteau).

0955-2219/$ – see front matter © 2007 Elsevier Ltd. All rights reserved.
doi:10.1016/j.jeurceramsoc.2007.02.190

liquid phase during the sintering of SiC. The compositions of the four powder batches were designed to yield 3.6 vol%, 7.3 vol%, 20 vol%, and 23.2 vol% YAG, respectively, in the sintered materials. After successive steps of powder mixing, drying, and deagglomeration, several pellets were then uniaxially pressed (Model C, Carver Inc., Wabash, IN) in a steel die (25 mm diameter) at 50 MPa pressure. The pellets were subsequently cold-isostatically pressed (CP360, AIP, Columbus, OH) at a pressure of 350 MPa. Individual pellets were embedded in powder beds inside graphite crucibles with screwable lids. The pellets were sintered in a graphite furnace (Model 1000-3560-FP20, Thermal Technology Inc., Santa Rosa, CA) at 1950 °C for 2, 5, or 7 h in flowing Ar-gas atmosphere (see Table 1). The sintered pellets were cleaned and lightly ground to remove any surface reaction layers and/or adhered packing powder.

2.2. Microstructural characterization

Densities of the sintered materials were measured using the Archimedes method, with distilled water as the immersion medium. Density values of 3.213 g cm^{-3} and 4.544 g cm^{-3} for SiC and YAG, respectively, were employed in the relative density calculations.

Polished cross-sections of the specimens were plasma-etched (PT 1750, Fissions Instruments, East Sussex, UK) for 100–120 min using $CF_4 + 4\%$ O_2 gas (300 Pa, 80 W) to reveal the grain boundaries, and were then observed under the SEM. Several micrographs of representative regions within the microstructures were recorded for grain size analysis. Image analysis was used to estimate the longest chord[15] (defined as the length l), the longest dimension perpendicular to the longest chord l (the width d), and the aspect ratio (l/d). For each sintered material at least 300 grains were used for the grain size analysis.

2.3. Mechanical properties characterization

2.3.1. Vickers indentation

Vickers-indentation tests (peak load $P_V = 98$ N) were performed on the polished specimens under ambient conditions using a hardness tester (Model MV-1, Matsuzawa, Tokyo, Japan). The indentation sites were examined using the optical microscope (Epiphot 300, Nikon, Tokyo, Japan), and the diagonals (a_V) and radial-crack diameters ($2c$) of each indent were measured using image analysis. The Vickers-indentation hardness (H) and toughness (K_{IC}) were calculated using $H = 2P_V/a_V^2$ and $K_{IC} = 0.016(E/H)^{0.5}P_V c^{-1.5}$, respectively.[16,17] Elastic modulus (E) values determined experimentally using Hertzian indentation (WC ball of radius 7.94 mm, peak loads in the range 15–400 N) were used in the K_{IC} calculations.

2.3.2. Sliding wear

Several polished disks (7 mm diameter, 2 mm thickness) were core-drilled from the sintered materials for wear testing. Wear testing was performed at room-temperature in a Falex multi-specimen tribometer (Faville-Le Vally Corp., Sugar Grove, IL) using the ball-on-three-disks geometry. Here, a commercial, bearing grade Si_3N_4 ball (NBD 200, Cerbec, East Granby, CT) of radius 6.35 mm rotated in contact with three disk specimens aligned with their surface normals in tetrahedral coordination relative to the rotation axis.[18] Paraffin oil (Heavy Grade, Fisher Scientific, Fair Lawn, NJ) was used as the lubricant (viscosity $\sim 3.4 \times 10^{-5}$ m^2 s^{-1} at 40 °C). The contact load on each disk was 70 N, which corresponds to an initial contact pressure of $\approx$1 GPa (elastic regime), and the rotation speed was 100 rpm, corresponding to a sliding velocity of $\sim$0.04 m s^{-1}. The wear tests were interrupted at intervals, and the diameters of the circular wear scars on each disk were measured under the optical microscope (two orthogonal measurements per disk, three disks per ceramic). The wear-scar diameter was used as quantification of the extent of wear damage. At the end, the wear damage was also observed under the scanning electron microscope, SEM (S-3600N, Hitachi, Japan).

3. Results and discussion

Fig. 1A–D are SEM micrographs representative of the four different microstructures selected in this work: fine-equiaxed-grained (Fig. 1A), fine-equiaxed-grained with a higher amount of intergranular phase (Fig. 1B), coarse-equiaxed-grained (Fig. 1C), and duplex with both elongated and equiaxed grains (Fig. 1D). The nomenclature, sintering conditions, microstructural parameters, and mechanical properties of these materials are summarized in Table 1. The absence of residual porosity in the SEM images indicates that the four ceramics are fully dense, which is consistent with the density values given in Table 1. Also, the contrast within the SiC grains represents the characteristic core–shell structure, evidence that grain growth took place by solution-precipitation (Ostwald ripening).[15,19] In these ceram-

Table 1
Properties of the six LPS SiC ceramics selected in this study

Ceramic[a]	vol.% YAG	Sintering time (h)	Density (mg m^{-3})	Density (%)	Grain length, l (μm)	Grain aspect ratio, l/d	Elastic modulus, E (GPa)	Hardness, H (GPa)	Toughness, K_{IC} (MPa m$^{0.5}$)
Eq-3.6YAG-0.8	3.6	2	3.261	100	0.8	1.4	410 ± 3	24.0 ± 0.6	2.4 ± 0.1
Eq-7.3YAG-0.8	7.3	2	3.310	100	0.8	1.4	390 ± 2	21.2 ± 0.3	2.9 ± 0.2
Eq-3.6YAG-2.0	3.6	7	3.228	99	2.0	1.4	405 ± 2	17.7 ± 0.5	3.9 ± 0.3
Dp-7.3YAG-2.0	7.3	7	3.310	100	2.0	2.0	391 ± 3	16.9 ± 0.4	4.0 ± 0.3
El-20.0YAG-3.1	20.0	5	3.479	100	3.1	4.0	350 ± 3	16.1 ± 0.4	3.9 ± 0.2
Eq-23.2YAG-0.8	23.2	2	3.523	100	0.8	1.4	345 ± 4	16.6 ± 0.3	2.8 ± 0.1

[a] x–yYAG–z, where x refers to grain morphology (Eq for equiaxed-grained microstructure, El for elongated-grained, and Dp for a duplex microstructure with both equiaxed and elongated grains), y the YAG content in vol.% and z refers to grain size in μm.

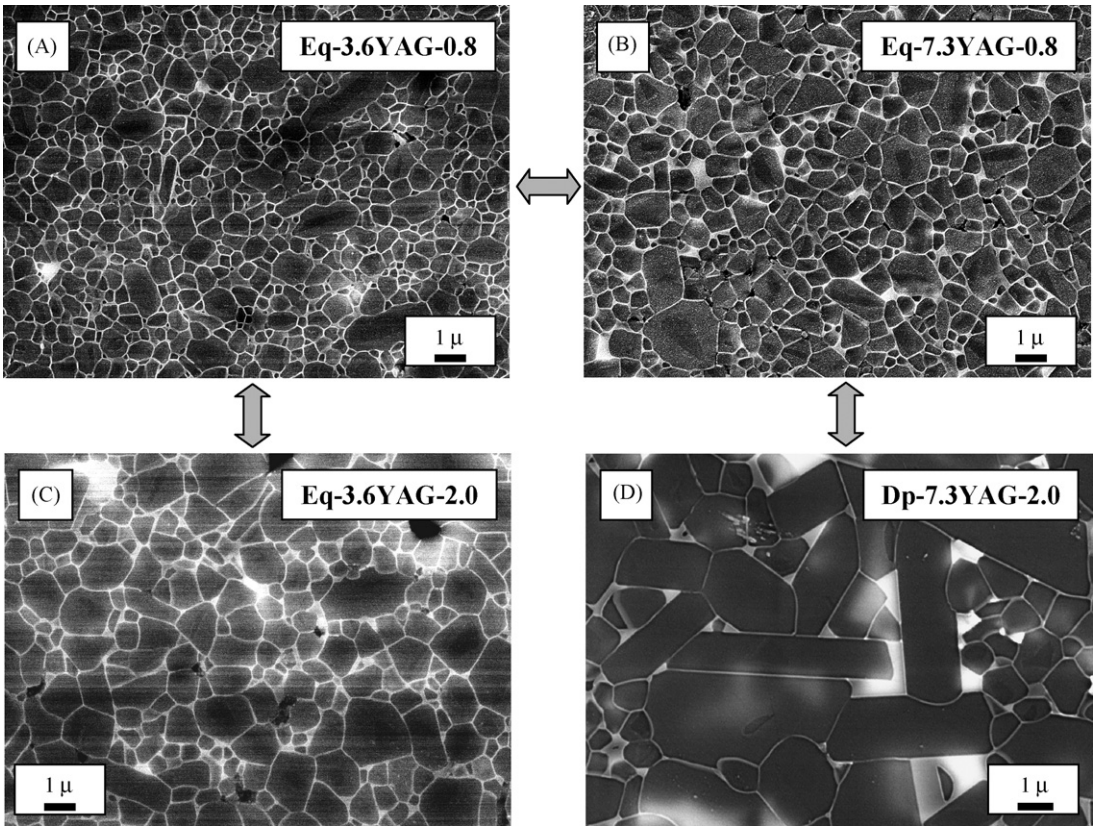

Fig. 1. SEM micrographs of polished and plasma-etched cross-sections of the four different microstructures selected in this study. The light region is crystalline YAG and the darker regions are SiC grains. Arrows relate the materials compared to illustrate the effect of the different microstructures on the sliding wear of LPS SiC.

ics, coarsening is interface-reaction controlled, since grain size is independent of the liquid-phase amount. Anisotropic coarsening occurred after 7 h sintering in the ceramic with 7.3 vol.% YAG as a result of 6H → 4H phase transformation.[20,21] Thus, there is a liquid phase threshold – 7.3 vol.% – below which elongated grain growth is hindered due to the proximity of the SiC grains.

Regarding the mechanical properties, the increase in the amount of softer intergranular phase resulted in a decrease in the elastic modulus and the hardness of the SiC/YAG composites, and in an increase in the fracture toughness due to enhanced crack deflection.[22] Obviously, grain coarsening did not affect the elastic modulus, and also led to a decrease in hardness due to easy shear-faulting along weak SiC/YAG interfaces[23–25] and high-temperature YAG degradation,[26] and to crack-wake-bridging toughening.[27]

The Eq-3.6YAG-0.8 and Eq-7.3YAG-0.8 ceramics (Fig. 1A and B) can be used to show the effect of the intergranular phase content on the sliding wear of LPS SiC (Fig. 2). These materials exhibit the characteristic two-stage wear-accumulation behavior that has been observed in other polycrystalline ceramics[1,7,8,18,28–30]: mild deformation-controlled wear, followed by severe fracture-controlled wear, with a well-defined wear transition. Assuming that for the two wear stages the wear-scar diameter evolves with sliding time according to the empirical expression $A + B \log t$, where t is cumulative sliding time in min, we calculated the rates of mild and severe wear (B) and the transition times in the ceramics (Table 2). Increasing the intergranular phase amount from 3.6 vol.% to 7.3 vol.%, we observed a two-fold increase in the mild-wear rate, and a five-fold and 2.6-fold decrease in the transition time and severe-wear rate, respectively. According to this, Eq-3.6YAG-0.8, which has

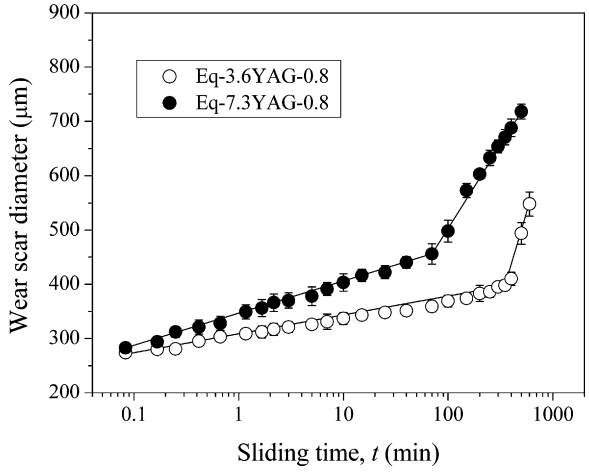

Fig. 2. Wear scar diameter as a function of the sliding time for selected LPS SiC ceramics to show the effect of the intergranular phase content on the sliding wear of LPS SiC. Common to all the wear plots: each datum point represents an average of three specimens tested; error bars represent data range. The solid lines are fits to the data, with the discontinuities in the lines indicating wear transitions.

Table 2
Wear properties and associated parameters for the six LPS SiC ceramics

Ceramic	Effective tensile residual stress, q (MPa)[a]	Pre-transition slope, m (μm)	Wear-transition time, t_c (min)	Post-transition slope, m (μm)
Eq-3.6YAG-0.8	53	30	350	769
Eq-7.3YAG-0.8	99	60	70	300
Eq-3.6YAG-2.0	53	60	135	273
Dp-7.3YAG-2.0	99	37	300	230
El-20.0YAG-3.1	210	15	310	370
Eq-23.2YAG-0.8	231	90	25	198

[a]The effective tensile residual stresses were calculated by[11]: $q = (V_f(1 - V_f)E\Delta\alpha\Delta T)/2$, where V_f is the volume fraction of the YAG phase, E the Young's modulus of the composite, $\Delta\alpha$ the thermal expansion mismatch ($\Delta\alpha \approx 5 \times 10^{-6}\,^{\circ}C^{-1}$) and ΔT is the temperature range through which the material is cooled without stress relaxation ($\Delta T \approx 1500\,^{\circ}C$).

the greatest hardness and the lowest toughness, is the most sliding-wear resistant ceramic here. Fig. 3 shows optical and SEM micrographs of a typical wear scar at the end of the wear tests, after 500 min of sliding. Grain-boundary fracture and grain pullout are clearly observed in the micrographs.

The effect of grain size on the sliding-wear of LPS SiC is illustrated in Fig. 4 using the Eq-3.6YAG-0.8 and Eq-3.6YAG-2.0 ceramics (Fig. 1A and C). The rates of mild and severe wear and the transition times are given in Table 2. Now there is a two-fold increase in the mild-wear rate, and a 2.6-fold and 2.8-fold reduction in the transition time and severe-wear rate, respectively, with increase in grain size from 0.8 μm to 2.0 μm. Again, Eq-3.6YAG-0.8 is the most sliding-wear resistant material. Similarly to the fine-grained ceramic, the wear damage in the coarse-grained ceramic consisted of grain-boundary fracture and grain pullout.

The above trend, that is, the decrease in the wear resistance with increasing grain size, is reversed when grain coarsening is accompanied by grain elongation, as confirmed in Fig. 5 by comparing the Eq-7.3YAG-0.8 and Dp-7.3YAG-2.0 ceramics (Fig. 1A and D). The development of elongated grains in Dp-7.3YAG-2.0 results in a decrease in both the mild- and severe-wear rates (1.6-fold and 1.3-fold, respectively), and in a significant delay in the wear transition (4.3-fold). Now the most sliding-wear resistant material (the material with elongated grains) has also the highest fracture toughness. Therefore, this type of *in situ* reinforced microstructure allows the classical trade-off between sliding-wear resistance and long-crack toughness in polycrystalline ceramics to be overcome.[13,14] In addition, Dp-7.3YAG-2.0 maintains a high degree of surface integrity compared to the equiaxed-grained ceramics at the end of the wear tests. Indeed, the wear damage in the Dp-7.3YAG-2.0 ceramic only consists of some pullout of the second phase, so

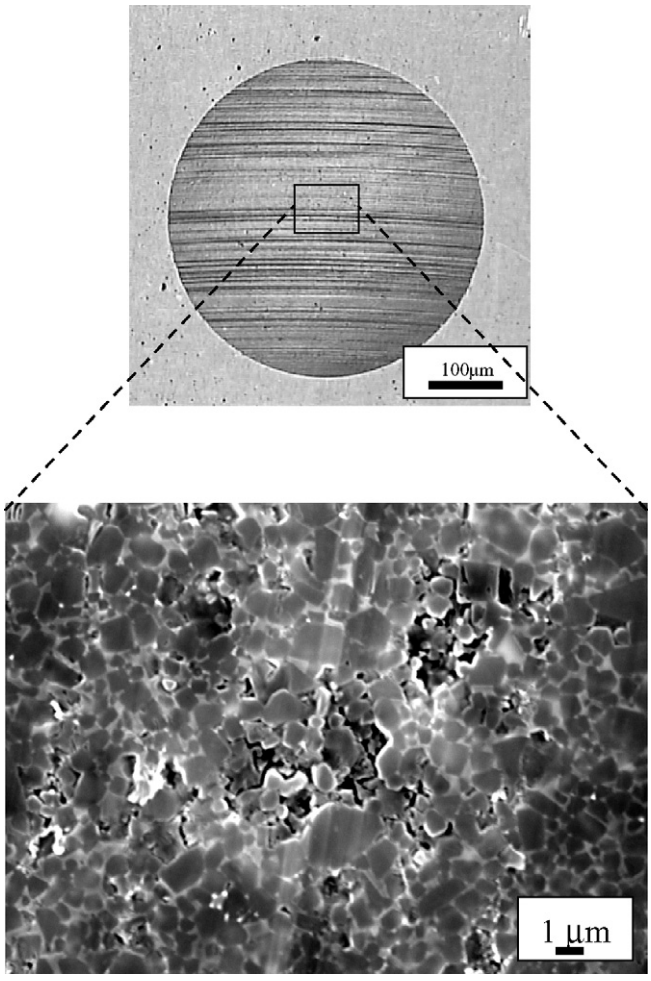

Fig. 3. Optical and SEM micrographs of the wear damage after 500 min of sliding in the Eq-7.3YAG-0.8 ceramic. The presence of grooves in the optical images is indicative of the fracture-controlled wear regime.

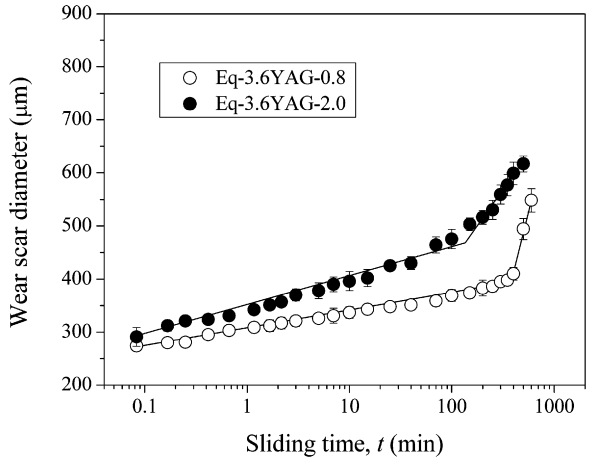

Fig. 4. Wear scar diameter as a function of the sliding time for selected LPS SiC ceramics to show the effect of grain size on the sliding wear of LPS SiC.

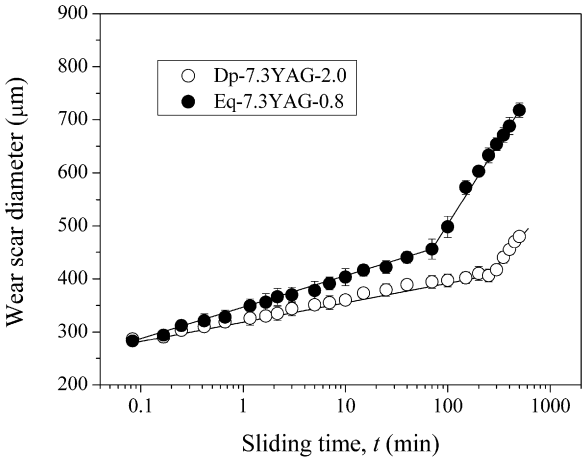

Fig. 5. Wear scar diameter as a function of the sliding time for selected LPS SiC ceramics to illustrate the effect of grain morphology on the sliding wear of LPS SiC.

that the interconnecting network of SiC grains remains in place after 1.2 km of sliding (see Fig. 6).

4. Analysis

A simple model due to Lawn and co-workers provides a framework for analyzing the sliding wear of these ceramics.[28] According to this model, during deformation-controlled wear, plastic-deformation damage (mainly dislocation pile-ups[7,8]) accumulates within the grains as a function of sliding time t, inducing tensile stresses ($\sigma_D(t)$) that bear up against the grain boundaries. In addition, tensile stresses from the thermal expansion mismatch (q) are also present. Values of q for the materials considered here are given in Table 2. The model then considers "penny"-shaped grain-boundary facet cracks of length βl under the wear contact, where l is the grain size and β is ≤ 1. Those short cracks are subjected to q and $\sigma_D(t)$, resulting in a time-dependent stress intensity factor for such cracks[28]:

$$K(t) = \left(\frac{2}{\pi^{0.5}}\right)(\sigma_D(t) + q)\beta l^{0.5}. \quad (1)$$

Despite the various assumptions and simplifications,[b] this model captures the trends in the sliding wear of the equiaxed-grained ceramics, in particular the effects of the intergranular phase amount and grain size. With increasing intergranular phase amount from 3.6 vol.% (Eq-3.6YAG-0.8 ceramic) to 7.3 vol.% (Eq-7.3YAG-0.8 ceramic), the hardness decreases (Table 1), and the tensile residual stress increases (Table 2). The decreasing hardness results in a higher rate at which the dislocation-plasticity induced stress accumulates, and hence a greater pre-transition wear rate; the increasing tensile residual stress will contribute to reducing the wear-transition time, qualitatively consistent with the results in Fig. 2. Likewise, with increasing grain size from 0.8 μm (Eq-7.3YAG-0.8 ceramic) to 2.0 μm (Eq-7.3YAG-2.0 ceramic), the hardness decreases resulting in a higher mild-wear rate. The increased grain size, while maintaining constant residual stress, will also assist in reducing the transition time according to Eq. (1), qualitatively consistent with the results in Fig. 4.

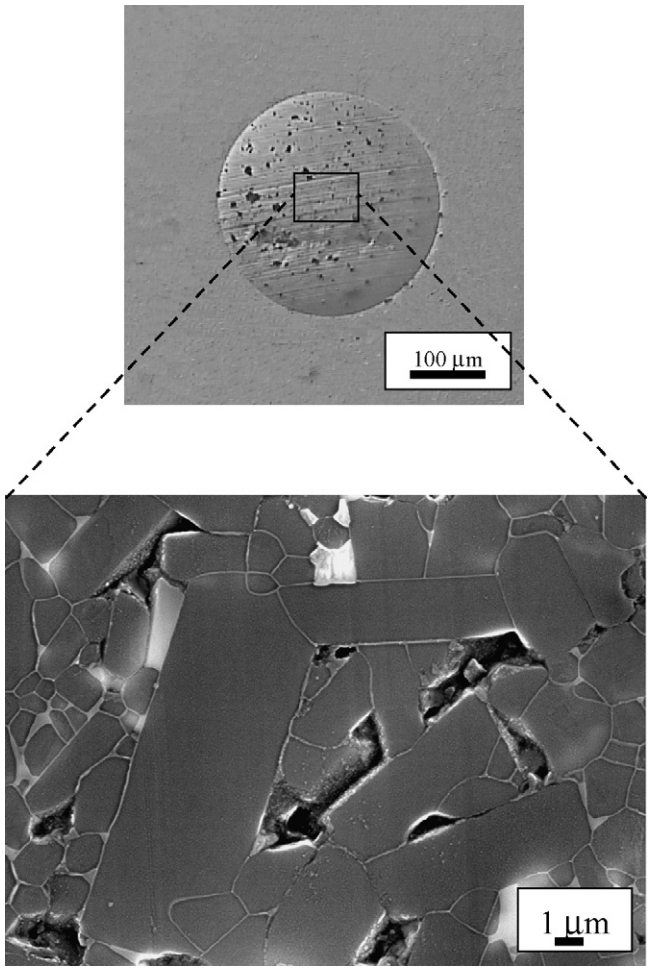

Fig. 6. Optical and SEM micrographs of the wear damage after 500 min of sliding in the Dp-7.3YAG-2.0 ceramic. The material maintains a high degree of surface integrity at the conclusion of the wear tests.

The above correlation between hardness and mild-wear rate breaks down in the case of highly heterogeneous ceramics such as Dp-7.3YAG-2.0, as observed in Fig. 5. Indeed, since mild wear is controlled by dislocation plasticity, one would expect Dp-7.3YAG-2.0 to have a greater mild-wear rate than Eq-7.3YAG-0.8, as it has a lower hardness. However, the reduced hardness in Dp-7.3YAG-2.0 is due to enhanced shear-faulting along grain boundaries, which is not likely to occur under the initial elastic contact in the wear tests. Therefore, the harder interlocking SiC-grain network in the elongated-grained ceramic appears to control the mild wear, with little contribution from the softer, isolated YAG phase which does not form

[b] First, the model assumes all grains and grain-boundary cracks to be of the same size, and the deformation and fracture events are not considered to be stochastic. Second, the grain pullout debris is likely to interfere during the wear test, which is not considered either. Third, the wear-stress accumulation rate is not likely to be linear because strain hardening is expected to occur. Fourth, the wear-stress accumulation rate may not be the same for the different materials considered here. Finally, the residual stresses may influence the strain hardening rate, which needs to be investigated further.

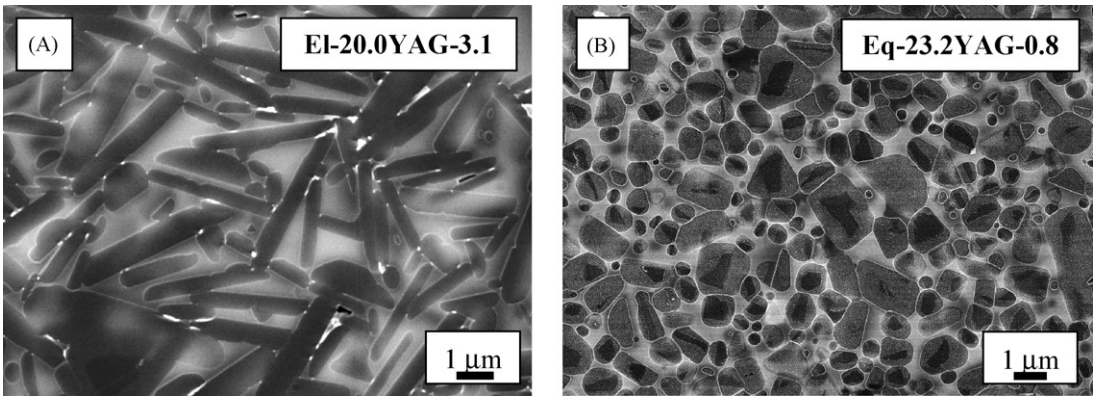

Fig. 7. SEM micrographs of polished and plasma-etched cross-sections of the El-20.0YAG-3.1 and Eq-23.2YAG-0.8 ceramics. The light region is crystalline YAG and the darker regions are SiC grains.

the continuous network that it does in the equiaxed-grained ceramics.

The results presented in this work suggest two different strategies for the microstructural design of sliding-wear resistant polycrystalline ceramics: (1) grain refinement, leading to fine-equiaxed-grained microstructures, and (2) grain elongation, leading to *in situ* toughened microstructures. Further improvements in the sliding-wear resistance of LPS SiC using the first strategy would require the use of a SiC starting powder with smaller particle size (nanosize powders), as well as a reduction in both the intergranular phase amount and the sintering duration and temperature. However, under these circumstances the conventional mechanical mixture of the starting powders (SiC plus additives) might not lead to a homogeneous distribution of the liquid phase, and the resulting materials will not be fully dense. One would have to explore the use of colloidal processing techniques, such as the sol–gel routine, as an alternative to introduce the sintering aids and thus overcome this drawback. For the optimization of the sliding-wear resistance of LPS SiC using the second strategy, a larger transformation-assisted anisotropic grain growth would be desirable, which can be achieved by using different combinations of SiC starting powders.

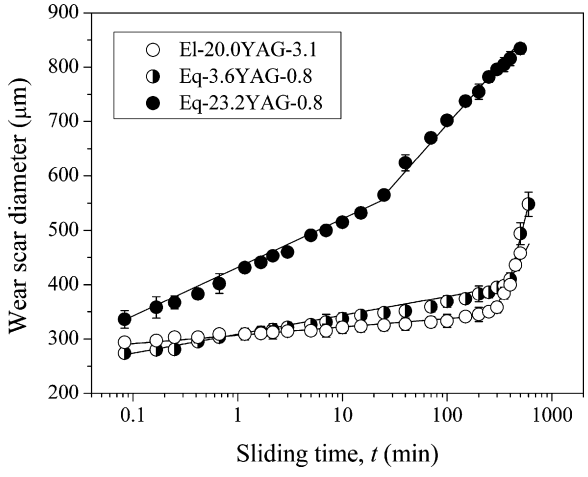

Fig. 8. Wear scar diameter as a function of the sliding time for selected LPS SiC ceramics to illustrate the optimized sliding-wear resistance in the El-20.0YAG-3.1 ceramic prepared from β-SiC powder.

As mentioned above, the *in situ* toughening approach has a clear advantage over the grain refinement strategy: it allows the fracture toughness of the materials to be simultaneously improved, resulting in ceramics with a superior combination of mechanical properties overall. We therefore have focused on optimizing the *in situ* toughening strategy by using β-SiC starting powder. β-SiC powders are more expensive than the more conventional α-SiC powders,[14] but they are more effective in promoting highly anisotropic grain growth due to the $\beta \rightarrow \alpha$ transformation during sintering.[15] The microstructure of a material obtained from β-SiC starting powder, El-20.0YAG-3.1, is shown in Fig. 7 and compared with an equiaxed-grained ceramic with a similar amount of intergranular phase. Note that the microstructure of the El-20.0YAG-3.1 ceramic is now unimodal, consisting only in elongated SiC grains, which results in an increased average aspect ratio (4.0). This optimized *in situ* toughened microstructure is much more sliding-wear resistant than its equiaxed-grained counterpart, as clearly observed in Fig. 8. Moreover, Fig. 8 shows that the El-20.0YAG-3.1 ceramic is even more sliding-wear resistant than the most resistant equiaxed-grained ceramic, Eq-3.6YAG-0.8, despite containing a much higher amount of intergranular phase; in addition, the elongated-grained material is more than 60% tougher.

5. Summary

We have reviewed the microstructure-properties relationship in the lubricated sliding-wear of pressureless liquid-phase-sintered (LPS) SiC ceramics under initial elastic contact. Based on this study, the following conclusions can be drawn:

- The increase in the content of intergranular phase and the grain coarsening degrade the sliding-wear resistance in LPS SiC ceramics.
- The transformation-assisted anisotropic coarsening of SiC grains improves the sliding-wear resistance in LPS SiC ceramics.
- Two strategies for the microstructural design of low-cost, sliding-wear resistant SiC-based ceramics are (1) grain refinement, and (2) grain elongation. The latter has the clear

advantage that it allows the fracture toughness to be simultaneously improved.
- The *in situ* toughening strategy for obtaining both sliding-wear resistant and tough LPS SiC ceramics can be optimized by using β-SiC starting powders.

Acknowledgements

Supported by the Ministerio de Ciencia y Tecnología (Government of Spain) and the Fondo Europeo de Desarrollo Regional (FEDER) under grant Nos. CICYT MAT 2004-05971, UNEX00-23-013 and UNEX05-23-037.

References

1. Wang, Y. S. and Hsu, S. M., Wear and wear transition mechanisms of ceramics. *Wear*, 1996, **195**, 112–122.
2. Wong, H. C., Umehara, N. and Kato, K., Frictional characteristics of ceramics under water-lubricated conditions. *Tribol. Lett.*, 1998, **5**, 303–308.
3. Kato, K., Wear in relation to friction—a review. *Wear*, 2000, **241**, 151–157.
4. Gahr, K.-H. Z., Blattner, R., Hwang, D.-H. and Pöhlmann, K., Micro- and macro-tribological properties of SiC ceramics in sliding contact. *Wear*, 2001, **250**, 299–310.
5. Hsu, S. M. and Shen, M., Wear prediction of ceramics. *Wear*, 2004, **256**, 867–878.
6. Wang, X. L., Kato, K. J. and Adachi, K., The critical condition for the transition from HL to ML in water-lubricated SiC. *Tribol. Lett.*, 2004, **16**, 253–258.
7. Cho, S.-J., Um, C.-D. and Kim, S.-S., Wear and wear transition in silicon carbide ceramics during sliding. *J. Am. Ceram. Soc.*, 1996, **79**, 1247–1251.
8. Cho, S.-J., Um, C.-D. and Kim, S.-S., Wear and wear transition mechanism in silicon carbide ceramics during sliding. *J. Am. Ceram. Soc.*, 1995, **78**, 1076–1078.
9. Sigl, L. S., Thermal conductivity of liquid phase sintered silicon carbide. *J. Eur. Ceram. Soc.*, 2003, **23**, 1115–1122.
10. Schlesinger, M. E., Melting points, crystallographic transformation and thermodynamic values. In *Engineered Materials Handbook*, *Vol 4*, ed. S. J. Schneider Jr. ASM International, 1991, pp. 883–891.
11. Borrero-Lopez, O., Ortiz, A. L., Guiberteau, F. and Padture, N. P., Effect of microstructure on sliding-wear properties of liquid-phase-sintered α-SiC. *J. Am. Ceram. Soc.*, 2005, **88**, 2159–2163.
12. Borrero-Lopez, O., Ortiz, A. L., Guiberteau, F. and Padture, N. P., Propiedades mecánicas a temperatura ambiente de cerámicos de α-SiC sinterizados con fase líquida de Y_2O_3–Al_2O_3. *Bol. Soc. Esp. Ceram. Vidrio*, 2005, **44**, 265–269.
13. Borrero-Lopez, O., Ortiz, A. L., Guiberteau, F. and Padture, N. P., Improved sliding-wear resistance in in situ-toughened silicon carbide. *J. Am. Ceram. Soc.*, 2005, **88**, 3531–3534.
14. Borrero-Lopez, O., Ortiz, A. L., Guiberteau, F. and Padture, N. P., Low-cost liquid-phase-sintered SiC with improved sliding-wear resistance. *J. Am. Ceram. Soc.*, 2007, **90**(2), 541–545.
15. Xu, H., Bhatia, T., Deshpande, S. A., Padture, N. P., Ortiz, A. L. and Cumbrera, F. L., Microstructural evolution in liquid-phase-sintered SiC. I. Effect of starting SiC powder. *J. Am. Ceram. Soc.*, 2001, **84**, 1578–1584.
16. Lawn, B. R., In *Fracture of Brittle Solids*. 2nd ed. Cambridge University Press, Cambridge, UK, 1993.
17. Anstis, G. R., Chantikul, P., Marshall, D. B. and Lawn, B. R., A critical evaluation of indentation techniques for measuring fracture toughness. I. Direct crack measurements. *J. Am. Ceram. Soc.*, 1981, **64**, 533–538.
18. Thompson, S. C., Pandit, A., Padture, N. P. and Suresh, S., Stepwise-graded Si_3N_4–SiC ceramics with improved wear properties. *J. Am. Ceram. Soc.*, 2002, **85**, 2059–2064.
19. Sigl, L. S. and Kleebe, H.-J., Core/rim structure of liquid-phase-sintered silicon carbide. *J. Am. Ceram. Soc.*, 1993, **76**, 773–776.
20. Tanaka, H. and Zhou, Y., Low temperature sintering and elongated grain growth of 6H-SiC powder with AlB_2 and C additives. *J. Mater. Res.*, 1999, **14**, 518–522.
21. Tanaka, H., Hirosaki, N., Nishimura, T., Shin, D.-W. and Park, S.-S., Nonequiaxial grain growth and polytype transformation of sintered α-silicon carbide and β-silicon carbide. *J. Am. Ceram. Soc.*, 2003, **86**, 2222–2224.
22. Borrero-Lopez, O., Ortiz, A. L., Guiberteau, F. and Padture, N. P., Effect of liquid-phase content on the contact mechanical properties of liquid-phase sintered α-SiC. *J. Eur. Ceram. Soc.*, 2007, **27**(6), 2521–2527.
23. Lawn, B. R., Padture, N. P., Cai, H. and Guiberteau, F., Making ceramics ductile. *Science*, 1994, **263**, 1114–1116.
24. Padture, N. P. and Lawn, B. R., Toughness properties of a silicon carbide with in situ-induced heterogeneous grain structure. *J. Am. Ceram. Soc.*, 1994, **77**, 2518–2522.
25. Padture, N. P. and Lawn, B. R., Contact fatigue of a silicon carbide with a heterogeneous grain structure. *J. Am. Ceram. Soc.*, 1995, **78**, 1431–1438.
26. Borrero-Lopez, O., Ortiz, A. L., Guiberteau, F. and Padture, N. P., Hardness degradation in liquid-phase sintered SiC with prolonged sintering. *J. Eur. Ceram. Soc.*, in press.
27. Padture, N. P., In situ-toughened silicon carbide. *J. Am. Ceram. Soc.*, 1994, **77**, 519–523.
28. Cho, S.-J., Hockey, B. J., Lawn, B. R. and Bennison, S. J., Grain-size and R-curve effects in the abrasive wear of alumina. *J. Am. Ceram. Soc.*, 1989, **72**, 1249–1252.
29. Cho, S.-J., Moon, H., Hockey, B. J. and Hsu, S. M., The transition from mild to severe wear in alumina during sliding. *Acta Metall. Mater.*, 1992, **40**, 185–192.
30. Wang, X., Padture, N., Tanaka, H. and Ortiz, A. L., Wear-resistant ultrafine-grained ceramics. *Acta Mater.*, 2005, **53**, 271–277.